Deubiquitinase USP5 regulates RIPK1 driven pyroptosis in response to myocardial ischemic reperfusion injury

Wenjing Sun[1,2], Hongquan Lu[3†], Lingkun Ma[1†], Cong Ding[1], Hailan Wang[4] and Yingjie Chu[1,4*]

Abstract

Background Gasdermin D (GSDMD) mediated pyroptosis plays a significant role in the pathophysiology of myocardial ischemia/reperfusion (I/R) injury. However, the precise mechanisms regulating pyroptosis remain unclear. In the study, we aimed to investigate the underlying mechanism of pyroptosis in myocardial I/R injury.

Methods In the present study, we analyzed the effects of USP5 on the RIPK1 kinase activity mediated pyroptosis in vitro after H/R (hypoxia/reoxygenation) and in vivo in a MI/R mouse model. TTC and Evan's blue dye, Thioflavin S and immunohistochemistry staining were performed in wild-type, RIPK1$^{flox/flox}$ Cdh5-Cre and USP5 deficiency mice. CMEC cells were transfected with si-USP5. HEK293T cells were transfected with USP5 and RIPK1 overexpression plasmid or its mutants. The levels of USP5, RIPK1, Caspase-8, FADD and GSDMD were determined by Western blot. Protein interactions were evaluated by immunoprecipitation. The protein colocalization in cells was monitored using a confocal microscope.

Results In this study, our data demonstrate that RIPK1 is essential for limiting cardiac endothelial cell (CMEC) pyroptosis mediated by caspase-8 in response to myocardial I/R. Additionally, we investigate the role of ubiquitin-specific protease 5 (USP5) as a deubiquitinase for RIPK1. Mechanistically, USP5 interacts with RIPK1, leading to its deubiquitination and stabilization.

Conclusions These findings offer new insights into the role of USP5 in regulating RIPK1-induced pyroptosis.

Keywords Ischemia/reperfusion, Microvascular injury, RIPK1, Pyroptosis, USP5

†Hongquan Lu and Lingkun Ma contributed equally to this work and should be considered joint first author.

*Correspondence:
Yingjie Chu
hnsycyj123@163.com
[1]Department of Cardiology, Henan Provincial People's Hospital, Zhengzhou University People's Hospital, No.7, Weiwu Road, Zhengzhou 450000, Henan Province, China
[2]Department of Clinical Microbiology, Henan Provincial People's Hospital, Zhengzhou University People's Hospital, Zhengzhou 450000, China
[3]Department of Nuclear Medicine, Third People's Hospital of Honghe State, Honghe 661000, China
[4]Department of Cardiology, Henan Provincial People's Hospital, Henan University People's Hospital, Zhengzhou 450000, China

Introduction

Acute myocardial infarction (AMI) remains a significant cause of worldwide mortality and morbidity [1]. While restoring blood flow to an ischemic organ prevents irreversible cellular injury, reperfusion alone often causes more tissue damage than ischemia [2]. Emerging studies have also shown that pyroptosis and inflammation play crucial roles in the pathophysiology of myocardial I/R injury [3, 4]. Pyroptosis, an inflammatory type of cell death characterized by gasdermins, is triggered by various stimuli and is closely associated with inflammasome activation [5]. However, the

regulatory mechanisms of pyroptosis are not fully understood.

Receptor-interacting protein kinase 1 (RIPK1), a serine/threonine kinase, is essential for cellular and tissue balance through the combination of inflammatory responses and signaling pathways for cell death, including apoptosis and necroptosis, which are involved in various physiological and pathological processes [6, 7]. The kinase activity of RIPK1 has been demonstrated to be essential in the progression of various inflammatory conditions such as neurodegenerative, inflammatory diseases, and nonalcoholic steatohepatitis [6, 8, 9]. Controlling the activation of RIPK1 kinase has been shown to effectively alleviate organ damage. However, its connection to myocardial I/R injury and microvascular dysfunction has not been thoroughly explored. In addition, it remains unclear whether RIPK1 activation mediates pyroptotic cell death. Based on these views, we hypothesize that RIPK1-mediated CMECs pyroptosis is involved in the pathophysiological processes of MI/R.

It is widely recognized that RIPK1's diverse functions can be regulated through various post-translational modifications, including ubiquitination and phosphorylation [10, 11]. Ubiquitination is a critical enzymatic cascade that maintaining cellular processes involves ensuring the proteins stability and their interactions. The regulation of protein homeostasis within cells is controlled by reversible processes known as ubiquitination and deubiquitination, which are governed by E3 ligases and deubiquitinating enzymes (DUBs) [12]. Several studies have reported mechanisms that promote RIPK1 ubiquitination and protein stability [13, 14]. However, the role of ubiquitin-specific protease 5 (USP5), a member of the USP protein family primarily responsible for dissociating unanchored polyubiquitin, in myocardial I/R injury has not been studied.

In this study, we demonstrate that USP5 mitigates CMEC pyroptosis by impairing RIPK1 kinase activity, and that USP5 in hematopoietic cells is responsible for the protective effects against I/R-induced pyroptosis. Furthermore, we reveal that USP5 inhibits RIPK1 kinase activity by removing K63-linked polyubiquitin chains from RIPK1, thereby suppressing caspase-8 activation and cell pyroptosis. The results of this study indicate that USP5 is crucial for preventing RIPK1-mediated caspase-8 activation to prevent CMECs pyroptosis. It suggests that USP5 plays a significant role in mitigating myocardial I/R injury. This research underscores the potential of targeting USP5 as a promising therapeutic approach for treating myocardial I/R injury.

Materials and methods
Mice
RIPK1 conditional knockout (cKO) mice were purchased from GemPharmatech Co., Ltd (Nanjing, China), which were established using CRISPR/Cas9 system. Cas9 mRNA, sgRNA and targeting vector containing LoxP sites were co-injected into fertilized eggs. Exons 3–6 were chosen as the conditional knockout region. Potential founders were verified by PCR and gene sequencing. RIPK1$^{flox/flox}$ mice were then mate to Cdh5-Cre transgenic mice (purchased from GemPharmatech Co., Ltd) to generate endothelial cell-specific RIPK1 conditional knockout mice (RIPK1$^{fl/fl}$ Cdh5-Cre). For animal experiments with 6-8-week-old RIPK1cKO mice, littermate control mice (RIPK1$^{flox/flox}$) were used. Primers employed for RIPK1 genotyping: F: 5′-3′GACAGCAACCCTGTAAAAGG; R: 5′-3′CGC ACTTCTGGGTGACACTA. *USP5* heterozygous-deficient mice (USP5 KO) were purchased from Cyagen Biosciences Inc (Suzhou, China), using CRISPR/Cas9 technique. USP5 KO mice and their representative WT control mice were maintained in specific-pathogen-free facility. Primers used for genotyping: F: 5′-3′CGCAGCATCAAGCAAGACAGGGG; R: 5′-3′TCA GAGTTAAAACTGGGTAT-GGG. All animal experiments were performed according to the Guideline for the Ethical Review Laboratory Animals, with the approval of the Scientific Investigation Board of Yunnan Bestai Biotechnology Co., Ltd (Kunming, Yunnan Province, China), and the protocol for sample collection was authorized by the Ethics Committee of the of Yunnan Bestai Biotechnology Co., Ltd (approval date 2023, code BST-MICE-PZ-20230426-01).

Anesthesia and euthanasia Sodium pentobarbital (0.3%) was use to induce anesthesia in mice (30 mg/kg). Euthanasia was accomplished by cervical dislocation.

Myocardial I/R model
Male Wild-type (WT) and USP5$^{+/-}$C57BL/6J mice (6 ~ 8 weeks old) suffered myocardial I/R as described previously [15]. The left anterior descending (LAD) coronary artery was ligated by knotting a 6−0 silk suture for 45 min. And then, the slipknot was released for 6 h to induce I/R injury model. In sham-operated animals, mice were performed with the same procedures without ligation.

Measurements of infarct size and area at risk
6 h after reperfusion, TTC and Evan's blue dye was performed to measure the the infarct size according to previous described [15]. The infarct size (IS) was pale, whereas the area at risk (AAR) was brick red. The myocardial sections were photographed digitally.

Subsequently, the images were analyzed using Image J, the AAR was calculated as a percentage of the LV, and the IS was calculated as a percentage of the AAR.

Measurement of no-reflow area

Thioflavin-S staining used to measure the no-reflow area according to previous described [15]. Briefly, at the end of the experiment (at 6 h of reperfusion), the same occlusion location of the LAD was reoccluded, followed by administration of 0.1 ml of 4% thioflavin-S via the inferior vena cava immediately for identification of the no-reflow zone. Subsequently, 0.1 ml of 3% Evan's blue was administrated via tail vein to dye the non-ischemic myocardium. The heart was isolated, froze on -80 °C refrigerator and quickly cut into five 2 mm thick slices. Slices were exposed to UV light (363 nm) using a UV transilluminator for digital imaging. Light blue indicates the reflow area, whereas areas with no-reflow was dark blue. And then, the images were calculated using Image J. Percentage no-reflow zone was expressed as a percentage of LV.

Echocardiography

Transthoracic echocardiography was conducted on mice utilizing a high-resolution micro-imaging system (Visual Sonics Vevo 2100, Fujifilm Visual Sonics, USA) was utilized to assess the structure and function of the heart. Standard two-dimensional M-mode evaluations were conducted 6 h post-I/R surgery on mice that were anesthetized using 2% isoflurane. The ejection fraction (EF) and fractional shortening (FS) were measured.

Immunohistochemistry

Briefly, paraformaldehyde-fixed and paraffin-embedded cardiac tissue was cut into 4 µm-thick sections. Slides were dehydrated with a graded ethanol series. Subsequently, Sections incubated with 0.3% hydrogen peroxide in PBS to quench endogenous peroxidase activity. And then, sections were blocked with 5% goat serum for 2 h, and incubated with the following primary antibodies overnight at 4 °C: rabbit anti-F4/80 (1:100, Proteintech), rabbit anti-CD68 antibody (1:100, Proteintech), rabbit anti-CD11b antibody (1:100, Abclonal), rabbit anti-CD31 antibody (1:100, Proteintech). The next day, after washing three times, sections were incubated with the anti-rabbit IgG horseradish peroxide and detected using diaminobenzidine tetrahydrochloride (DAB) reaction, and then counterstained with Mayer's hematoxylin. Captured images were analyzed using Image J Software.

Cell culture

Primary CMECs were isolated from mice as previously described [16]. Briefly, Hearts were collected from the 6-week-old adult male mice and finely minced after removing the atria and right ventricle tissues. CMECs were separated by incubation with collagenase II (0.2%, Sigma) at 37 °C for 20 min, followed by incubation with trypsin (0.25%, Sigma) for 8–10 min. CMECs were collected after centrifuging at 1000 g for 5 min and resuspended in DMEM (Hyclone, Logan, UT, USA) supplemented with 10% FBS (BI: Israel, Middle East) and 100 IU/ml penicilin and 100 mg/ml streptomycin (Hyclone, Logan, UT, USA) and cultured at 37 °C with 5% CO2 in DMEM. The isolated CMECs were characterized using immunofluorescence with specific antibodies against CD31 (1:100, cell signaling technology) and Factor VIII (1:100, abcam).

Human cardiac microvascular endothelial cells (HCMECs) were obtained from ScienCell (Santiago, USA, Cat. No. 6000) and HEK293T cells were obtained from the Bei Na Chuang-lian Biotechnology (BNCC, Wuhan, China). The cells were cultivated at 37 °C under 5% CO2 in DMEM (Hyclone, Logan, UT, USA) supplemented with 10% FBS (BI: Israel, Middle East) and 100 U/ml penicilin and 100 mg/ml streptomycin (Hyclone, Logan, UT, USA).

Cell treatment

1 µg/ml tumor necrosis factor-α (TNFα, Sigma) was added to CMECs or HEK293T cells for 1 h to stimulate cell inflammation and cell death. For CMECs, briefly, oxygen-glucose deprivation injury (OGD/R) was established by incubating CMECs in a hypoxic chamber (1% O_2, 5% CO_2, 94% N_2) without serum medium for 2 h. Then the cells exchanged for complete DEME medium with serum and reoxygenated in the incubator containing CO_2 at 37 °C for 2 h.

Western blot analysis and immunoprecipitation

The process of western blot was described in our previous study [15]. Total protein was extracted from cells or cardiac tissues. Protein concentration was measured by the BSA protein assay (Thermo Fisher, USA). Proteins were separated by SDS-PAGE and then transferred onto PVDF membranes. The membranes were blocked with 5% non-fat milk and incubated overnight at 4 °C with the following primary antibodies: RIPK1 (1:1000, Proteintech), Caspase-8 (1:1000, abclonal), FADD (1:1000, Proteintech), GSDMD (1:1000, Abcam), c-GSDMD (1:1000, Abcam), NLRP3 (1:1000, Adipogen), Caspase-1 (1:1000, Adipogen), Caspase-4 (1:1000, abclonal) and GAPDH (1:5000, Proteintech). After washing three times with TBST, membranes were incubated with secondary HRP-conjugated IgG anti-mouse or anti-rabbit antibody for 2 h at room temperature. Proteins were visualized by ECL procedure (Bio-Rad, Hercules, CA). The expression levels of

target proteins were normalized using either β-actin or GAPDH as controls.

For immunoprecipitation (IP), cells were lysed with Cell Lysis Buffer (Absin, China) supplemented with a protease inhibitor (MCE, USA) on ice for 15 min. After centrifugation at 12,000×g for 15 min, the supernatant was incubated with IP antibodies for 1 h and together with protein A/G-magnetic beads (Santa cruz Biotechnology, USA) overnight at 4 ℃. After three times washing with IP buffer, immunoprecipitates were added to 40 μl 2 x loading buffer for boiling at 100 ℃ for 5 min. Then extracts were separated by SDS-PAGE and analyzed by immunoblot with specific antibodies.

For vitro binding assay, cells were subjected to lysis using 500 μl of IP buffer, followed by shearing with a sonication apparatus, and then centrifuged at 12,000 g for 15 min at a temperature of 4 ℃. The supernatants were subsequently incubated overnight at 4 ℃ with the suitable antibody, either anti-Flag magnetic beads (MCE, HY-K0207) or anti-Myc magnetic beads (MCE, HY-K0206). Immunoprecipitants were gathered through centrifugation at 3,000 g for 3 min at 4 ℃, after which the beads were washed three times using 500 μl of IP buffer. An aliquot of 40 μl of 2 × Laemmli sample buffer was mixed with the beads, and the samples were then subjected to SDS-PAGE for resolution.

In vitro ubiquitination assays

For the in vitro ubiquitination assay, Flag-RIPK1 and HA-Ub, HA- K48 (K48), HA-K63 (K63), together with WT or C335A mutant Myc-USP5, were transfected into HEK293T cells for 24 h. Then, HEK293T cells were treated with the proteasome inhibitor MG132 (Selleck,) for another 6 h. Cells were lysed in 150 μl cell lysis buffer (Absin, China) with 5 mM N-ethylmaleimide (NEM) and complete protease inhibitor mixture (Selleck, S2619), and centrifuged at 12,000 g at 4 ℃ for 15 min. 20% cells were lysed in loading buffer for input and the remaining supernatants were then incubated with anti-Flag magnetic beads (MCE, HY-K0207), or anti-Myc magnetic beads (MCE, HY-K0206) overnight at 4 ℃, and the beads were then washed three times with 500 μl of IP buffer. Immunoprecipitants were collected by centrifugation at 12,000 g at 4 ℃ for 1 min. An aliquot (40 μl) of 2×Laemmli sample buffer was added to the beads. Samples were resolved by SDS-PAGE.

Immunofluorescence staining and confocal analysis

CMECs seeded on confocal dish were immersed in 4% paraformaldehyde solution for 15 min, followed by permeabilization in 0.1% Triton X-100 for another 15 min. Subsequently, the cells underwent blocking with normal goat serum for 1 h. Following three times washes, the cells were treated with primary antibodies: mouse anti-USP5 (1:200, Proteintech) and rabbit anti-RIPK1 (1:200, ABclonal) overnight at 4 ℃. Cells were washed with PBS for three times, and then incubated with secondary antibody (Alexa Fluor 488 goat anti-mouse IgG or Alexa Fluor 594 goat anti-rabbit IgG) for 1 h at room temperature. Nuclei were stained with DAPI (Thermo Fisher, USA). Confocal images were acquired using a Confocal microscopy (Olympus, Tokyo, Japan) for detection of colocalization.

Plasmids and transfection

Expression vectors for HA-Ub WT, mutant K48 and mutant K63 plasmids were kindly provided by Dr Wei Zhao (Shan Dong University, Shandong, China). The full length of human USP5 were cloned into the pcDNA3.4/myc-plasmid (Stratagene). Full length and deletion mutants of human USP5 were constructed using pFlag-CMV-MCS. The full length of human RIPK1 were cloned into the pcDNA3.1/Flag-plasmid (Stratagene). Full length and deletion mutants of human RIPK1 were constructed using pFlag-CMV-2. Transient transfections were carried out using lip3000 according to the manufacturer's instructions, into HEK293T cells.

Caspase-1 and Caspase-8 activity

Caspase-1 and caspase-8 activity both in cells and in mice serum were assessed using caspase-1 and caspase-8 assay kit according to the manufacturer's instructions (Beyotime, C1101, C1151). And then the activation of caspase-1 and caspase-8 was measured at 405 nm using a microplate reader (ThermoFisher, USA), and the activity of caspase-1 and caspase-8 was subsequently calculated.

Lactate dehydrogenase release assay

The Lactate Dehydrogenase Release Assay Kit (Beyotime Biotechnology, China) was utilized to measure the concentration of LDH in serum from mice. The procedure was conducted following the manufacturer's guidelines. The levels of LDH were determined using a standard curve.

In vitro matrigel tube formation assay

Plates with 96 wells were initially coated with 50 μl of Matrigel and then incubated for 30 min at 37 ℃ with 5% CO2. Subsequently, HUVECs were subjected to trypsinization and then resuspended in the conditioned medium obtained from various treated CMECs at a concentration of 4×10^4 cells/ml. A volume of 100 μl of this cell suspension was placed into the angiogenesis slide, followed by an incubation period of 6 h at 37 ℃ in a 5% CO2 atmosphere. The total

lengths of tubes per field were quantified using ImageJ software.

Statistical analysis

All numerical data were presented as means ± SD. Statistical analysis was calculated with GraphPad Prism 9. Kolmogorov-Smirnov test was used to test for the distribution of variables. Statistical analysis was performed using a two-unpaired *student's t*-tests for single measured variable, one-or two-way ANOVA for multiple comparisons. $P < 0.05$ was deemed statistically significant. Animal survival analysis was analyzed by a log-rank test.

Results

USP5 as a positive regulator for RIPK1 kinase activation and pyroptosis

To investigate the effect of USP5 during RIPK1 kinase activation and pyroptosis, the expression of USP5, RIPK1 signaling pathway associated proteins and GSDMD were first detected in CMECs subjected to 2 h hypoxia followed 2 h re-oxygenation or stimulated by TNF-α. The protein levels of USP5, RIPK1, FADD and GSDMD were increased in CMECs subjected to 2 h hypoxia followed 2 h re-oxygenation and stimulated by TNF-α (Supplementary Fig. 1A-B, $P < 0.05$).

To elucidate the physiological functions of USP5, a specific and efficient small interfering RNA (siRNA) targeting USP5 was designed and transfected into human CMECs. The knockdown efficiency of siRNA was assessed at the protein level (Supplementary Fig. 2A-B, $P < 0.05$). And then, we initially detect the effect of USP5 on RIPK1 at the mRNA level. Our result showed that regulatory effect on RIPK1 mRNA expression was not influenced by USP5 knockdown (Supplementary Fig. 3A-B). However, caspase-8 activity was significantly reduced in USP5-silenced CMECs stimulated by TNF-α or subjected to H/R or in USP5 deficiency mouse serum (Fig. 1A-B, $P < 0.05$). Conversely, the activity of caspase-1 was unaffected by USP5 knockdown in mouse CMECs or in mouse serum (Fig. 1A-B, $P < 0.05$). Furthermore, HEK293T cells were transfected with Myc-tagged USP5. Similarly, increased expression of RIPK1 and GSDMD was observed in HEK293T cells upon USP5 overexpression (Fig. 1C-D, $P < 0.05$).

RIPK1 kinase activity is a critical step for caspase-8 activation to promote cell death. However, whether RIPK1-mediated cell death involves caspase-8-induced cleavage of GSDMD was unclear. Therefore, the effects of USP5 on caspase-8 activation and the expression of GSDMD were investigated. Interestingly, reduced the expression of RIPK1, caspase-8, and GSDMD was observed in both mouse and human CMECs subjected

to H/R upon USP5 knockdown and deficiency (Fig. 1E-H, $P < 0.05$). Additionally, the inhibitory of USP5 knockdown on pyroptosis after H/R was reversed by RIPK1 overexpression (Fig. 1I-J, $P < 0.05$). Altogether, USP5 exhibits a previously unrecognized destructive capability in CMECs following MI/R injury, likely by promoting RIPK1 kinase activation medicated pyroptosis.

USP5 interacts with RIPK1

To further elucidate how USP5 regulates RIPK1 activation, we initially investigated whether USP5 interacts with RIPK1. In vitro binding assays demonstrated a direct interaction between USP5 and RIPK1 (Fig. 2A). We then examined whether USP5 interacts with other components of complex II. Co-immunoprecipitation (Co-IP) assays in HEK293T cells expressing myc-tagged USP5 and Flag-tagged Caspase-8 or FADD showed an interaction between USP5 and RIPK1, but not with Caspase-8 or FADD (Fig. 2C). Furthermore, endogenous USP5-RIPK1 association was confirmed by Co-IP in CMECs under both normoxia and hypoxia-reoxygenation (H/R) conditions (Fig. 2B). Confocal microscopy also revealed colocalization of USP5 with RIPK1 (Fig. 2D).

USP5, a member of the ubiquitin-specific protease family, contains three critical domains: the zinc finger ubiquitin-specific protease (ZnF-UBP) domain, the ubiquitin-specific processing domain (USP), and the ubiquitin-associated (UBA) domain [14]. To determine which domain(s) of USP5 are responsible for the interaction with RIPK1, we generated a series of Myc-tagged USP5 truncated mutants (Fig. 2G). Co-IP results showed that RIPK1 could coprecipitate with USP5 wild type (WT), as well as mutants lacking the UBA or ZnF-UBP domain, but not with mutants lacking the USP domain or containing the USP5^{C335A} mutation (Fig. 2H). These findings suggested that the USP domain of USP5 mediates its interaction with RIPK1. Additionally, we constructed three truncated mutants of RIPK1 (Fig. 2E). Co-IP experiments with these mutants indicated that the RIPK1 mutant lacking the kinase domain failed to bind with USP5, while mutants lacking the RHIM or death domain retained the ability to interact with USP5 (Fig. 2F). These results demonstrate that USP5 interacts with RIPK1 through the USP domain on USP5 and the kinase domain on RIPK1.

USP5 inhibits autophagic degradation of RIPK1

Considering USP5's role as a positive regulator of RIPK1 and its interaction with RIPK1, we hypothesized that USP5 promotes RIPK1 activation by impeding RIPK1 protein degradation. Indeed, USP5 knockdown significantly reduced RIPK1 expression in
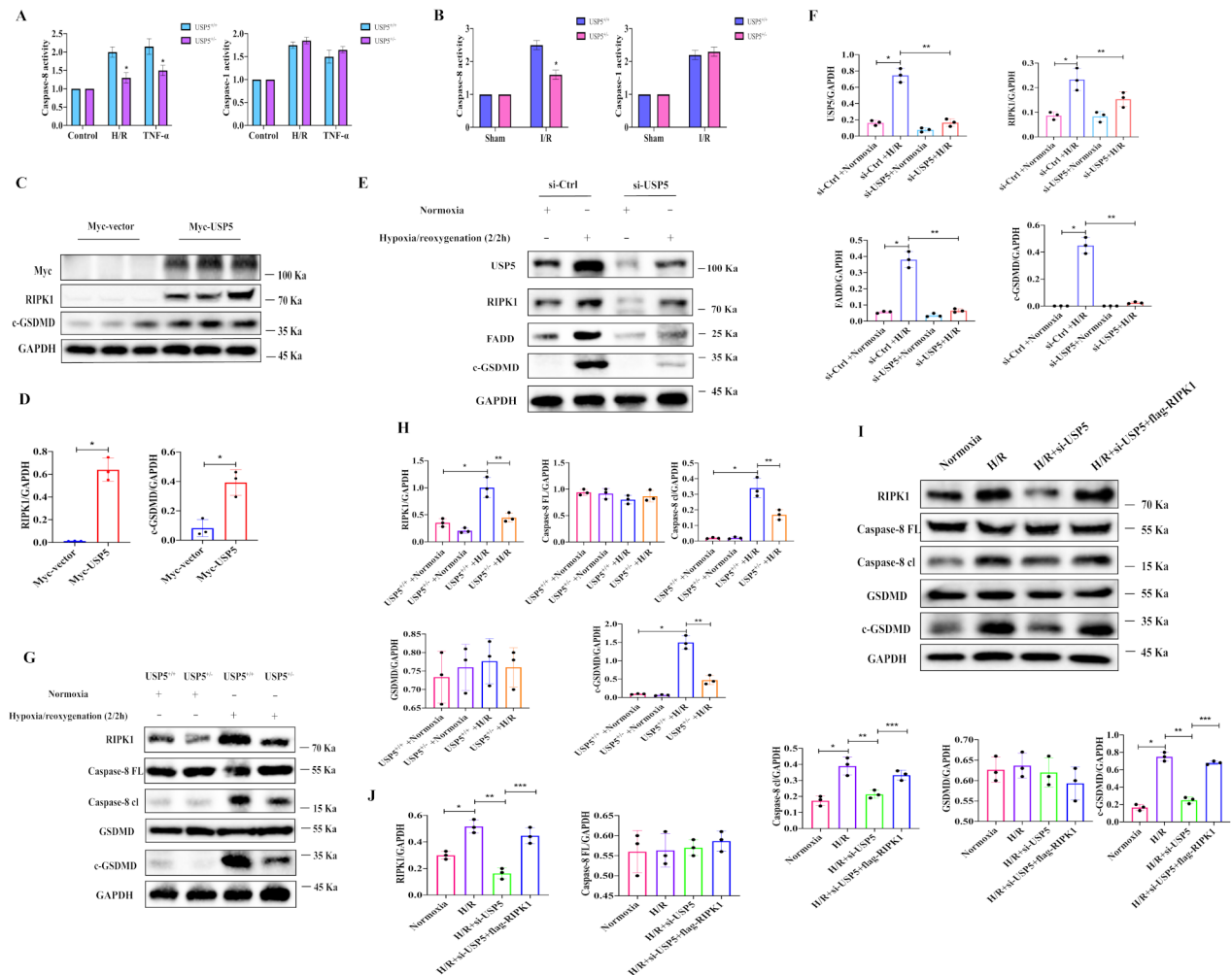
Fig. 1 USP5 as a positive regulator for RIPK1 kinase activation and pyroptosis. (**A**) Caspase-1 and Caspase-8 activity was determined by an enzyme activity assay kit in CMECs. Data are expressed as mean ± SEM ($n = 5$), and were analyzed using two-tailed Student *t* test. $^*P < 0.05$ vs. Control group. (**B**) Caspase-1 and Caspase-8 activity was determined by an enzyme activity assay kit in mouse serum. Data are expressed as mean ± SEM ($n = 5$), were analyzed using two-tailed Student *t* test. $^*P < 0.05$ vs. Sham group. (**C-D**) Immunoblot analysis and quantification by densitometry of RIPK1 and c-GSDMD protein in HEK293T cells transfected with Myc-USP5. Data are expressed as mean ± SD ($n = 3$), and were analyzed using Mann-Whitney *U* test or two-tailed Student *t* test. $^*P < 0.05$ vs. Myc-USP5 group. (**E-F**) Immunoblot analysis and quantification by densitometry of USP5, RIPK1, FADD and c-GSDMD protein in CMECs silenced of USP5. Data are expressed as mean ± SD ($n = 3$), and were analyzed using Mann-Whitney *U* test or two-tailed Student *t* test. $^*P < 0.05$ vs. H/R group. (**G-H**) Immunoblot analysis and quantification by densitometry of RIPK1, Caspase-8, GSDMD and c-GSDMD in mouse CMECs from USP5$^{+/+}$ or USP5$^{+/-}$ mice under normoxia or 2 h hypoxia/2 h reoxygenation. Data are expressed as mean ± SD ($n = 3$), and were analyzed using Mann-Whitney *U* test or two-tailed Student *t* test. $^*P < 0.05$ vs. H/R group, $^{**}P < 0.05$ vs. USP5$^{+/-}$+H/R group

mouse CMECs (Fig. 3A-B, $P < 0.05$). However, USP5 knockdown had no effect on RIPK1 mRNA expression in mouse CMECs (Fig. 3A). Similarly, USP5 knockdown notably decreased RIPK1 expression in human CMECs subjected to H/R or stimulated with TNF-α (Fig. 3C-D, $P < 0.05$), while it did not affect RIPK1 mRNA expression in human CMECs under H/R or stimulated with TNF-α (Fig. 3C). Importantly, similar results were observed in USP5-deficient mouse CMECs. USP5 deficiency significantly reduced RIPK1 expression in CMECs under both normoxia and H/R (Fig. 3E-F, $P < 0.05$). However, USP5 deficiency did not

affect NLRP3 and Caspase-1 expression (Fig. 3E-F, $P > 0.05$).

To investigate whether USP5 regulates RIPK1 degradation, CMEC cells were treated with the protein synthesis inhibitor cycloheximide (CHX) for varying durations. The results showed that RIPK1 protein degradation was accelerated in USP5 siRNA-transfected CMECs compared to control siRNA-transfected CMECs (Fig. 3G-H, $P < 0.05$). However, no differences in caspase-8, FADD, and NLRP3 protein degradation were observed between control siRNA and USP5 siRNA-transfected CMECs (Fig. 3G-H, $P > 0.05$). Subsequently, we investigated the degradation pathway of
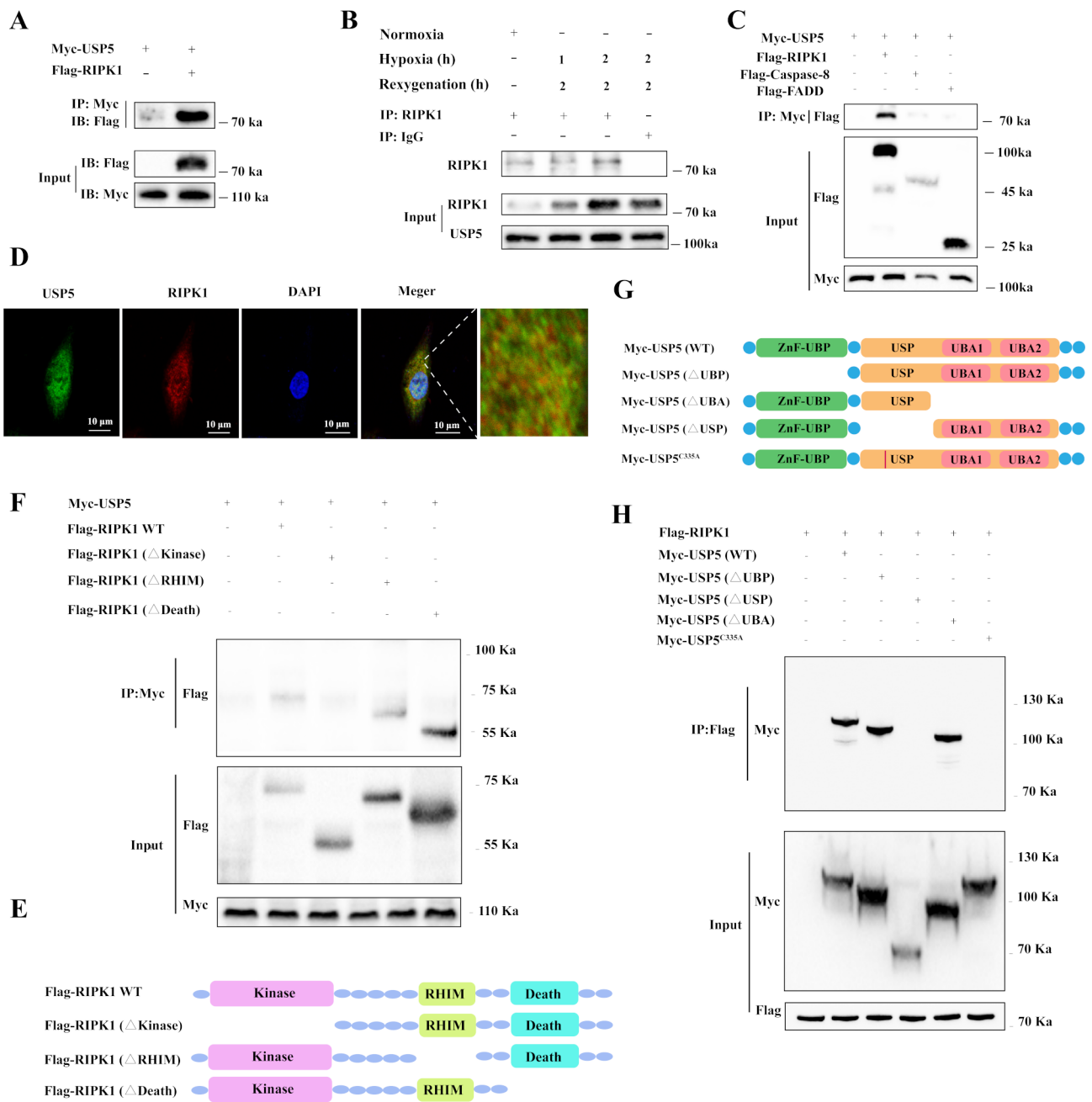
Fig. 2 USP5 interact with RIPK1. (**A**) Myc-tagged USP5 and Flag-tagged RIPK1were obtained by in vitro transcription and translation. Interaction between USP5 and RIPK1 was assayed by mixing USP5 and RIPK1 together followed by IP with Myc antibody and immunoblot analysis with Flag antibody. (**B**) Co-immunoprecipitation of endogenous USP5 with endogenous RIPK1 from CMECs under normoxia or hypoxia/reoxygenation for indicated time periods. (**C**) HEK293T cells expressing Myc-USP5 and Flag-RIPK1, Flag-caspase-8 or Flag-FADD were lysed. Co-immunoprecipitation of Myc-USP5 with Flag-RIPK1, Flag-caspase-8 or Flag-FADD from HEK293T cells. (**D**) Representative images of immunofluorescence staining of USP5 (green) and RIPK1 (red) were fixed in CMECs and incubated with a secondary antibody conjugated to Alexa Fluor 594 and Alexa Fluor 488. Colocalization between USP5 and RIPK1was examined by Confocal microscopy, Scale bar = 25 μm. (**E**) Schematic diagram of RIPK1and its truncation mutants. (**F**) Flag-tagged RIPK1or its mutants and Myc-USP5 were individually transfected into HEK293T cells. The cell lysates were immunoprecipitated with an anti-Flag antibody and then immunoblotted with the indicated antibodies. (**G**) Schematic diagram of USP5 and its truncation mutants. (**H**) Myc-tagged USP5 or its mutants and Flag-RIPK1 were individually transfected into HEK293T cells. The cell lysates were immunoprecipitated with an anti-myc antibody and then immunoblotted with the indicated antibodies. Data are representative of three independent experiments with similar results
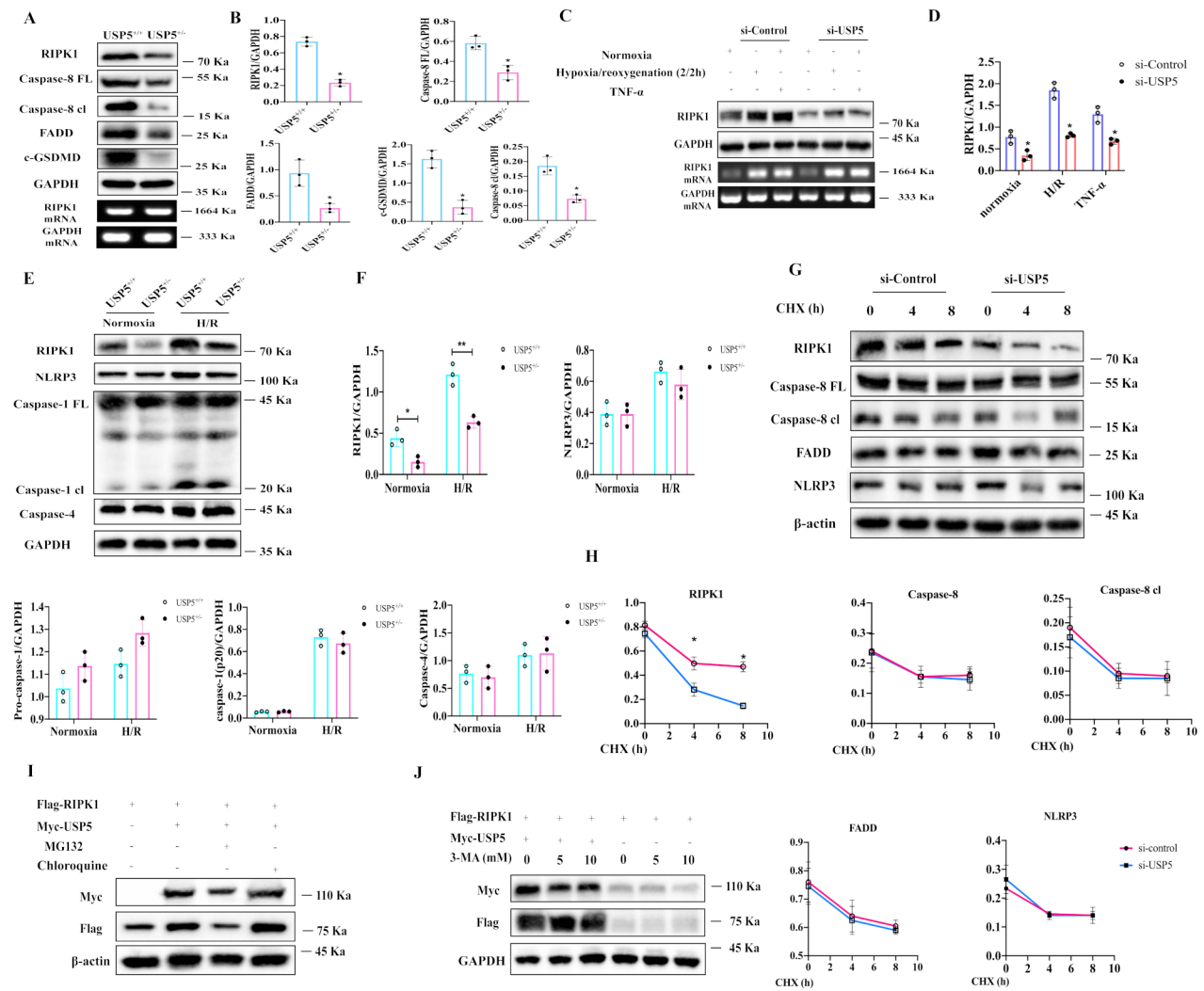
Fig. 3 USP5 deficiency promotes lysosomal degradation of RIPK1. (**A-B**) Immunoblot analysis and quantification by densitometry of RIPK1, Caspase-8, FADD and c-GSDMD protein or RT-PCR analysis of mouse CMECs silenced of USP5. Data are expressed as mean ± SD ($n=3$), and were analyzed using Mann-Whitney U test or two-tailed Student t test. *$P<0.05$ vs. USP5^{+/+}group. (**C-D**) Immunoblot analysis and quantification by densitometry of RIPK1, protein or RT-PCR analysis of HCMECs silenced of USP5, then under normoxia or 2 h hypoxia/2 h reoxygenation and stimulated for TNF-α for 1 h. Data are expressed as mean ± SD ($n=3$), and were analyzed using Mann-Whitney U test or two-tailed Student t test. *$P<0.05$ vs. si-Control group. (**E-F**) Immunoblot analysis of and quantification by densitometry of RIPK1, NLRP3, Caspase-1, and caspase-4 protein from USP5^{+/+} or USP5^{+/-} mouse CMECs under normoxia or 2 h hypoxia/2 h reoxygenation. Data are expressed as mean ± SD ($n=3$), and were analyzed using Mann-Whitney U test or two-tailed Student t test. *$P<0.05$ vs. USP5^{+/+}+normoxia group, **$P<0.05$ vs. USP5^{+/+}+H/R group. (**G-H**) Immunoblot analysis of extracts from HCMECs, and then treated for various times with cycloheximide (CHX). RIPK1, Caspase-8 FADD and NLRP3 expression levels were quantitated by measuring band intensities using 'ImageJ' software. (**I**) Immunoblot analysis of extracts from HEK293T cells transfected with Myc-USP5 and Flag-RIPK1 expression plasmid then treated with MG132 (10 mM) or chloroquine (10 mM) for 2 h. (**J**) Immunoblot analysis of extracts from HEK293T cells transfected with Myc-USP5 and Flag-RIPK1 expression plasmid then treated with 3-MA as indicated for 2 h

RIPK1 mediated by USP5. The suppression of RIPK1 degradation by USP5 could be reversed by the autophagy inhibitors 3-MA or chloroquine, but not by the proteasome inhibitor MG-132 (Fig. 3I) or the autophagy inhibitor 3-MA alone (Fig. 3J), indicating that USP5 inhibits RIPK1 degradation in the autophagy-lysosomal pathway.

USP5 reverses K63-linked ubiquitination of RIPK1

The ubiquitin system plays a pivotal role in controlling RIPK1 kinase activation. USP5 regulates multiple cellular processes dependent on its deubiquitinase activity. Given its identification as a RIPK1-associated protein, we investigated whether USP5 maintains RIPK1 stability through its enzymatic activity. Co-transfection of RIPK1 with HA-ubiquitin and WT-USP5 into HEK293T cells resulted in a significant decrease in RIPK1 ubiquitination in the presence of the USP5

expression plasmid (Fig. 4A). Importantly, the USP5 point mutation (C335A), which substitutes the cysteine residue with alanine at position 335 within the USP domain, lost the ability to suppress polyubiquitination of RIPK1 (Fig. 4A), indicating that USP5 inhibits RIPK1 ubiquitination through the USP domain. RIPK1 can be ubiquitinated with both K48 and K63 linkages in cells. To investigate which forms of ubiquitin chains on RIPK1 are affected by USP5, HEK293T cells were transfected with the ubiquitin mutant K48 and K63, which contain arginine substitutions of all lysine residues, except for the one at positions 48 and 63 respectively. USP5 significantly enhanced RIPK1 polyubiquitination in cells transfected with K48 ubiquitin, while no effect was observed in cells transfected with K63 ubiquitin (Fig. 4B), indicating that USP5 mediates K63-linked deubiquitination of RIPK1.

Under normal physiological circumstances, endogenous RIPK1 exhibited significant ubiquitination with both K48 and K63 connections following TNF-α induction (Fig. 4C). Nevertheless, in USP5-deficient CMECs, the K48-linked polyubiquitination of RIPK1 was nearly entirely eliminated, whereas the K63-linked ubiquitination remained unaffected. To further identify the ubiquitination sites in RIPK1 regulated by USP5, a series of RIPK1 mutants were constructed. However, USP5 mutants lacking the USP domain and C335A, which removes the deubiquitination activity, lost the ability to suppress the degradation of RIPK1 (Fig. 4D-E). These data suggest that USP5 specifically removes K63-linked polyubiquitin chains from RIPK1.
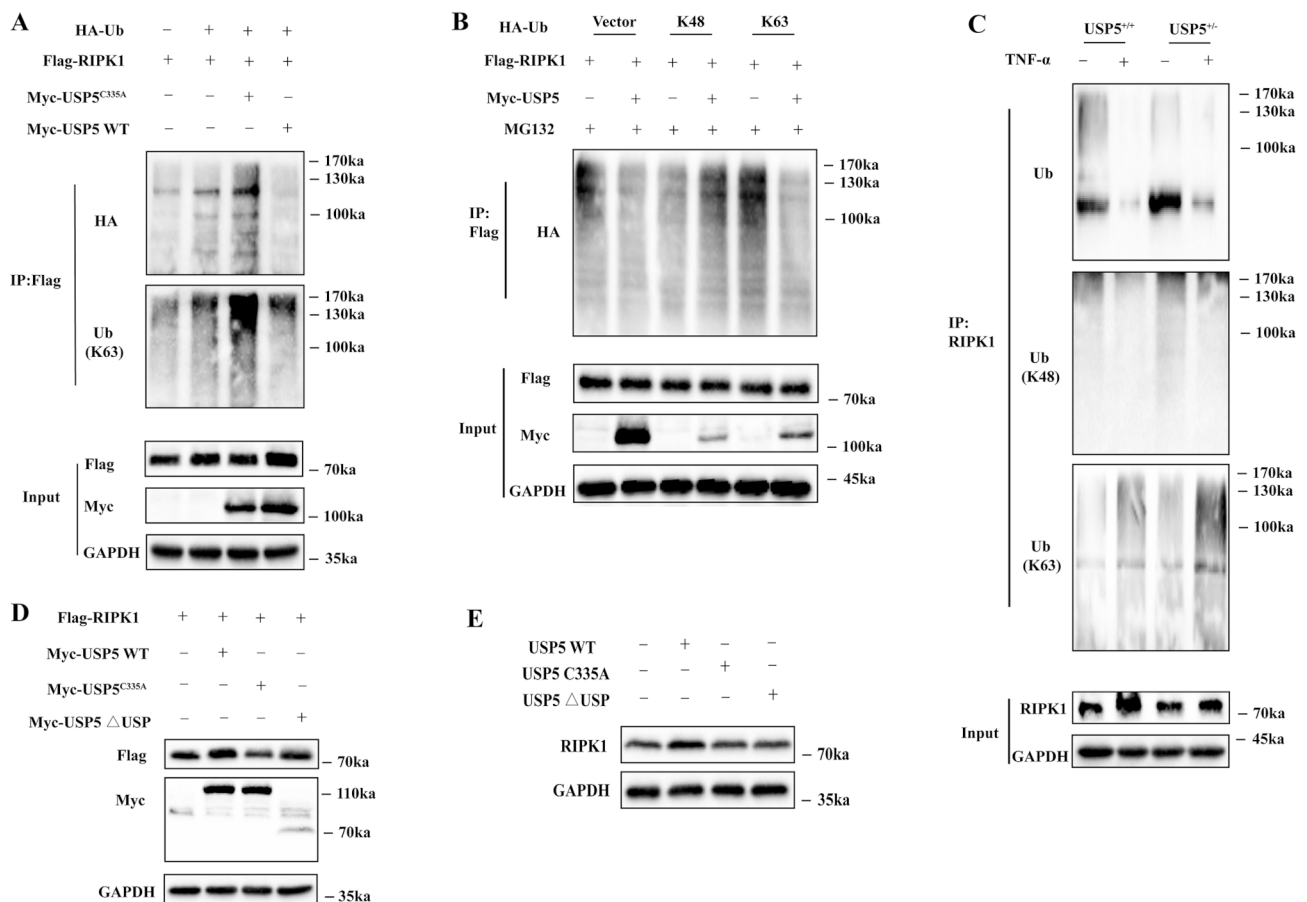

Fig. 4 USP5 reverses K63-linked ubiquitination of RIPK1. (**A**) Immunoblot analysis of lysates from HEK293T cells transfected with HA-tagged ubiquitin (HA-Ub), Flag-RIPK1and USP5 WT or C335A, followed by IP with anti-flag, probed with anti-HA or K63-Ub. (**B**) Immunoblot analysis of lysates from HEK293T cells transfected with HA-tagged K48-linked ubiquitin (K48-Ub) or HA-tagged K63-linked ubiquitin (K63-Ub), Flag-RIPK1 and Myc-USP5, followed by IP with anti-Myc, probed with anti-HA. (**C**) Immunoblot analysis of lysates from USP5$^{+/+}$/USP5$^{+/-}$mouse CMECs, followed by IP with anti-RIPK1, probed with anti-Ub, K48-Ub or K63-Ub. (**D**) Immunoblot analysis of extracts from HEK293T cells transfected with Flag-RIPK1and Myc-tagged USP5 or its mutants. (**E**) Immunoblot analysis of extracts from HCMECs transfected with USP5 wild type (WT), USP5 C335A or mutants of USP5. Similar results were obtained in three independent experiments

Sun *et al. Cell Communication and Signaling*   (2024) 22:466

Page 10 of 14

RIPK1 deficiency alleviates myocardial reperfusion injury in mice

To further explore the role of RIPK1 in myocardial microvascular reperfusion injury in mice, we generated *RIPK1^flox* mice with mice expressing the lysozyme promoter-driven Cre recombinase (Cdh5-Cre), resulting in conditional RIPK1 deletions (Cdh5-Cre$^+$/*RIPK1^{flox/flox}*) mice. Subsequently, we induced a myocardial I/R injury model in mice (45 min of ischemia followed by 6 h of reperfusion). Figure 5A depicts the effect of *RIPK1^{flox/flox}* on myocardial infarct size 6 h after reperfusion. In the *RIPK1^{flox/flox}* I/R group, the ratio of infarct size to area at risk (AAR) was found to be smaller compared to the WT-I/R group (Fig. 5B, *P* < 0.05). Additionally, the AAR as a percentage of the left ventricle (AAR/LV) was significantly reduced in the *RIPK1^{flox/flox}* I/R group (Fig. 5B, *P* < 0.05). Microvascular injury was assessed by microvascular permeability and the no-reflow phenomenon (Fig. 5C). In the *RIPK1^{flox/flox}* I/R group, the no-reflow area caused by I/R was found to be significantly reduced when compared to the WT-I/R group (Fig. 5D, *P* < 0.05). Moreover, *RIPK1^{flox/flox}* mice exhibited increased animal survival and attenuated infiltration of F4/80$^+$ and CD68$^+$ macrophages, as well as CD11b$^+$ neutrophils in the heart compared to the WT group (Fig. 5E-G, *P* < 0.05).

Furthermore, to confirm the role of RIPK1 in myocardial pyroptosis by regulating caspase-8 activity in vivo, the expression of related proteins was determined by western blot. The results demonstrated that *RIPK1^{flox/flox}* could downregulate the expression of Caspase-8, FADD, and cleaved-GSDMD in the heart (Fig. 5H-I, *P* < 0.05). Together, our findings suggest that RIPK1 deficiency inhibits pyroptosis and inflammatory cell accumulation in the heart following myocardial reperfusion in vivo. Additionally, LDH activity in mice serum from *RIPK1^{flox/flox}* + I/R group was significantly decreased compared with USP5$^{+/+}$ + I/R group (Fig. 5J, *P* < 0.05). We also found that RIPK1$^{flox/flox}$ versus WT showed higher CD31 density (Fig. 5K-L, *P* < 0.05). Meanwhile, tube formation of HUVECs was induced in si-RIPK1 versus controls under H/R conditions (Supplementary Fig. 4).

Ablation of USP5 largely inhibits RIPK1 induced myocardial reperfusion injury in mice

To further elucidate the role of USP5 in regulating myocardial reperfusion injury, USP5 knockdown mice were generated. Figure 6A illustrates the effect of USP5$^{+/-}$ on myocardial infarct size at 6 h after reperfusion. The infarct size/area at risk (IS/AAR) ratio of USP5-deficient mice was smaller following 45 min of ischemia and 6 h of reperfusion compared to WT mice

(Fig. 6B, *P* < 0.05). Moreover, the AAR as a percentage of the left ventricle (AAR/LV) in USP5-deficient mice was significantly decreased compared with WT mice (Fig. 6B, *P* < 0.05). To evaluate the effect of USP5 on microvascular injury, the no-reflow phenomenon was assessed (Fig. 6C). The no-reflow area induced by I/R was significantly reduced in USP5-deficient mice compared to WT mice (Fig. 6D, *P* < 0.05). Compared with WT mice, USP5 knockdown resulted in increased animal survival following 45 min of ischemia and 6 h of reperfusion (Fig. 6E, *P* < 0.05). Echocardiographic findings indicated a significant reduction in EF% and FS% following MI/R; however, this was restored with the knockdown of USP5 (Fig. 6F-G, *P* < 0.05). Our data also revealed that USP5 knockdown downregulated the expression of RIPK1, caspase-8, and cleaved-GSDMD in the heart (Fig. 6H-I, *P* < 0.05). Additionally, LDH activity in mice serum from USP5$^{+/-}$ + I/R group was significantly decreased compared with USP5$^{+/+}$ + I/R group (Fig. 6J, *P* < 0.05). Our study also found that USP5 knockdown promoted capillary formation, as evidenced by an increased capillary density assessed through immunohistochemistry analysis of the endothelial marker CD31 (Fig. 6K-L, *P* < 0.05). Furthermore, in the context of USP5 knockdown, we observed that si-USP5, compared to the control, induced tube formation under hypoxia/reoxygenation (H/R) conditions. (Supplementary Fig. 5). More importantly, Collectively, these findings suggest that USP5 plays crucial roles in inhibiting RIPK1 kinase activity and pyroptosis, thereby USP5 knockdown can alleviate myocardial or microvascular injury induced by MI/R. Taken together, these findings suggested that USP5 regulates cell pyroptosis by specifically deubiquitinating RIPK1 (Fig. 7).

Discussion

Cell death is a key mechanism contributing to the pathophysiology of MI/R injury. Recently, pyroptosis, a regulated form of programmed cell death, has emerged as a crucial player in MI/R injury [17]. In the present study, we demonstrate a significant role of USP5 in positively regulating pyroptosis by inhibiting RIPK1 kinase activation, rather than the inflammasome-dependent activation of caspase-1, which promotes pyroptosis. Importantly, we show that deficiency in both USP5 and RIPK1 leads to increased animal survival, attenuation of microvascular injury, and reduction in myocardial infarct size following myocardial ischemia-reperfusion.

RIPK1 is a protein with multiple domains, including a kinase domain, an intermediate domain, and a death domain (DD) [6]. Numerous reports suggest that RIPK1 kinase activity mediates the activation
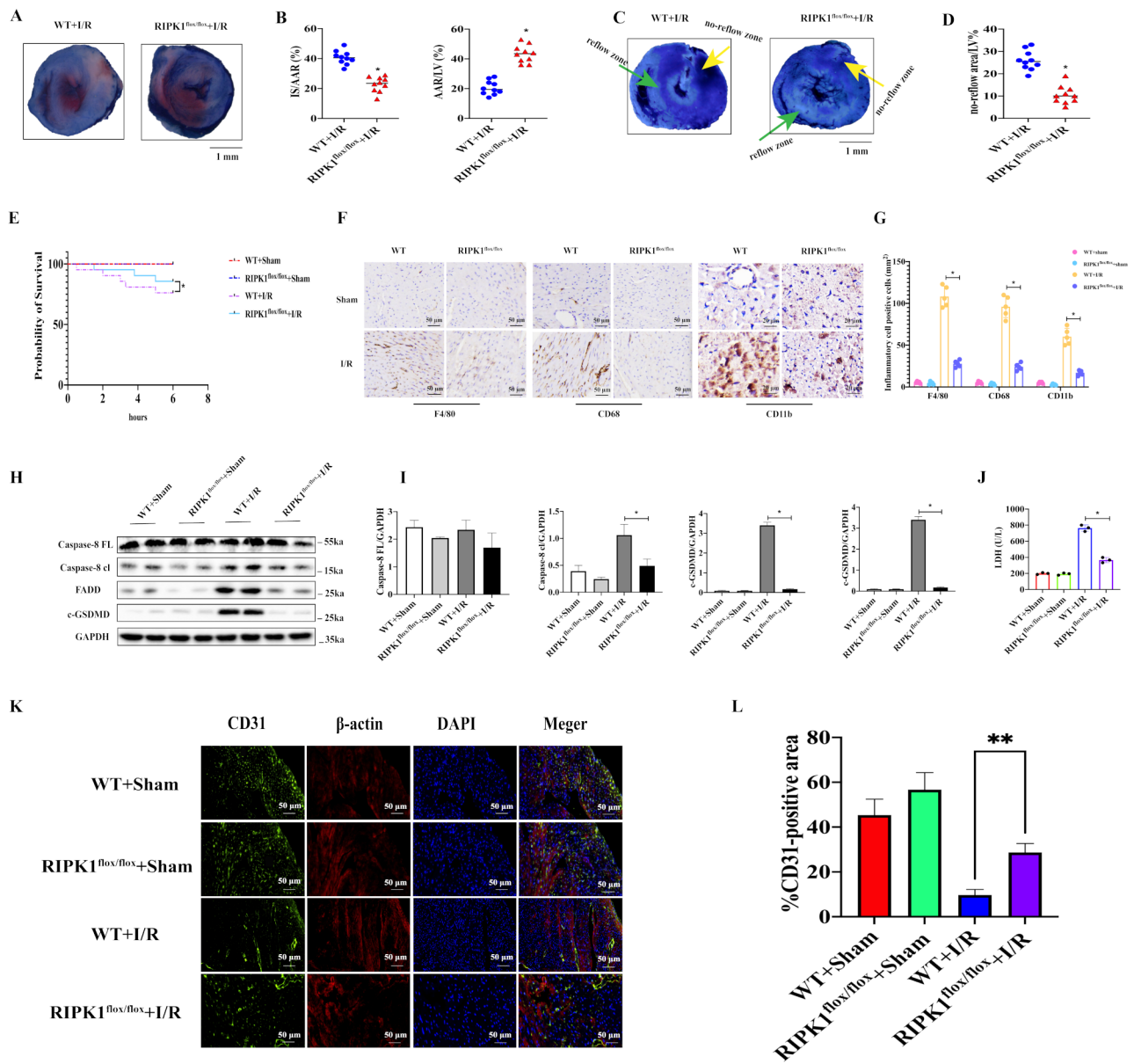
Fig. 5 RIPK1 alleviates myocardial reperfusion injury in mice. (**A**) Representative TTC-Evan's Blue stained sections of heart from each group. Brick red-stained area represents the area at risk (AAR), whereas the white area indicates the infarcted size (IS). (**B**) Ratio of AAR/LV, IS/ARR. Data are expressed as mean ± SD (*n* = 10 for each), and were analyzed using Mann-Whitney *U* test. *P < 0.05 vs. WT + I/R group. (**C**) Representative cross-sectional images of the left ventricular (LV) showing no-reflow regions indicated by the absence of thioflavin-S fluorescence within the ischemic area that consists of both no-reflow (yellow arrows) and reflow zones (green arrows) following IR. (**D**) Ratio of no reflow area/LV. Data are expressed as mean ± SD (*n* = 10 for each), and were analyzed using Mann-Whitney *U* test. *P < 0.05 vs. WT + I/R group. (**E**) Survival analysis for mice subjected to 45 min ischemia and following 6 h perfusion. (*P < 0.05 vs. WT + I/R group, Kruskal Wallis test with Dunn post-hoc test for survival analysis). (**F**) Heart sections were obtained from WT and RIPK1$^{flox/flox}$ mice under sham or 45 min ischemia and following 6 h reperfusion. The sections were immunohistologically analyzed by staining with antibody against F4/80, CD68 and CD11b. (**G**) Quantitative analysis of inflammatory cells was performed. Data are expressed as mean ± SD (*n* = 5 for each), were analyzed using Mann-Whitney *U* test or two-tailed Student *t* test. *P < 0.05 vs. WT + I/R group, Scale bar = 20 μm and 25 μm. (**H-I**) Immunoblot analysis and quantification by densitometry of Caspase-8, FADD and c-GSDMD in the heart from RIPK1$^{flox/flox}$ mice post-myocardial reperfusion. Data are expressed as mean ± SD (*n* = 3), were analyzed using Mann-Whitney *U* test or two-tailed Student *t* test. *P < 0.05 vs. WT + I/R group. (**J**) LDH activity in serum from WT, RIPK1$^{flox/flox}$, WT + I/R, RIPK1$^{flox/flox}$+I/R groups, *P < 0.05 vs. WT + I/R group. (**K-L**) Percent CD31-positive area per field was obtained by image processing using ImageJ. Data are expressed as mean ± SD (*n* = 3), were analyzed using Mann-Whitney *U* test or two-tailed Student *t* test. **P < 0.05 vs. WT + I/R group. Scale bar = 50 μm

Sun *et al. Cell Communication and Signaling*   (2024) 22:466
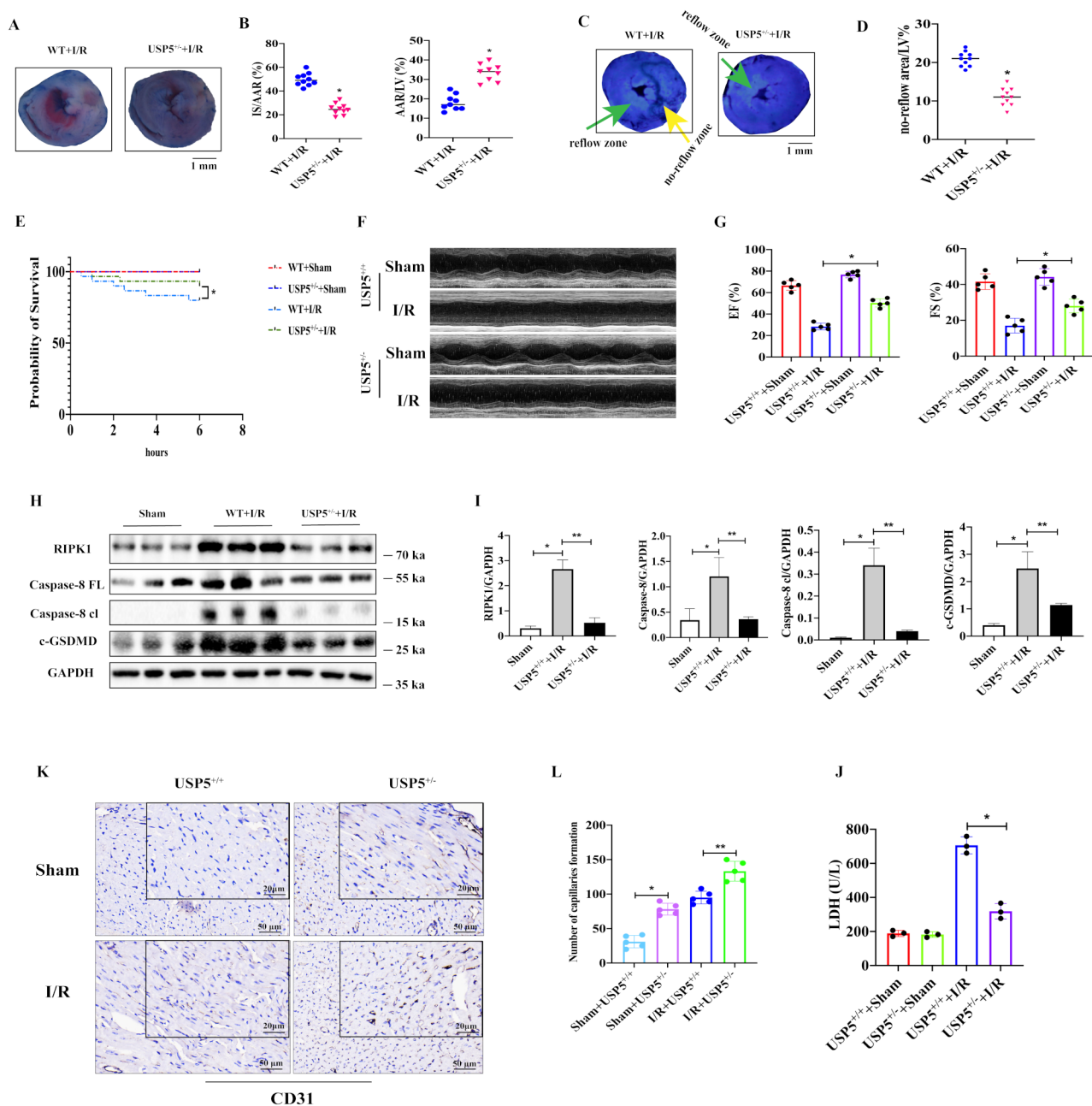
Page 12 of 14

Fig. 6 USP5 deficiency mitigates myocardial reperfusion injury in mice. (**A**) Representative TTC-Evan's Blue stained sections of heart from each group. Brick red-stained area represents the area at risk (AAR), whereas the white area indicates the infarcted size (IS). (**B**) Ratio of AAR/LV, IS/ARR. Data are expressed as mean ± SD ($n = 10$ for each), and were analyzed using Mann-Whitney U test. $^*P < 0.05$ vs. USP5$^{+/+}$ +I/R group. (**C**) Representative cross-sectional images of the left ventricular (LV) showing no-reflow regions indicated by the absence of thioflavin-S fluorescence within the ischemic area that consists of both no-reflow (yellow arrows) and reflow zones (green arrows) following IR. (**D**) Ratio of no reflow area/LV. Data are expressed as mean ± SD ($n = 10$ for each), and were analyzed using Mann-Whitney U test. $^*P < 0.05$ vs. USP5$^{+/+}$ +I/R group. (**E**) Survival analysis for mice subjected to 45 min ischemia and following 6 h perfusion ($^*P < 0.05$ vs. USP5$^{+/+}$ +I/R group, Kruskal Wallis test with Dunn post-hoc test for survival analysis). (**F-G**) Images of echocardiography of mice and quantitative analysis of EF% and FS%. (**H-I**) Immunoblot analysis and quantification by densitometry of RIPK1, Caspase-8 and c-GSDMD in the heart from USP5$^{+/-}$ mice post-myocardial reperfusion. Data are expressed as mean ± SD ($n = 3$), were analyzed using Mann-Whitney U test or two-tailed Student t test. $^*P < 0.05$ vs. USP5$^{+/+}$ +I/R group. (**J**) LDH activity in serum from USP5$^{+/+}$, USP5$^{+/-}$, USP5$^{+/+}$ +I/R, USP5$^{+/-}$ +I/R, $^*P < 0.05$ vs. USP5$^{+/+}$ +I/R group. (**K**) Heart sections were obtained from USP5$^{+/+}$ and USP5$^{+/-}$ mice under sham or 45 min ischemia and following 6 h reperfusion. The sections were immunohistologically analyzed by staining with antibody against CD31. (**L**) Quantitative analysis of inflammatory cells was performed. Data are expressed as mean ± SD ($n = 5$ for each), were analyzed using Mann-Whitney U test or two-tailed Student t test. $^*P < 0.05$ vs. USP5$^{+/+}$ +I/R group, Scale bar = 20 µm
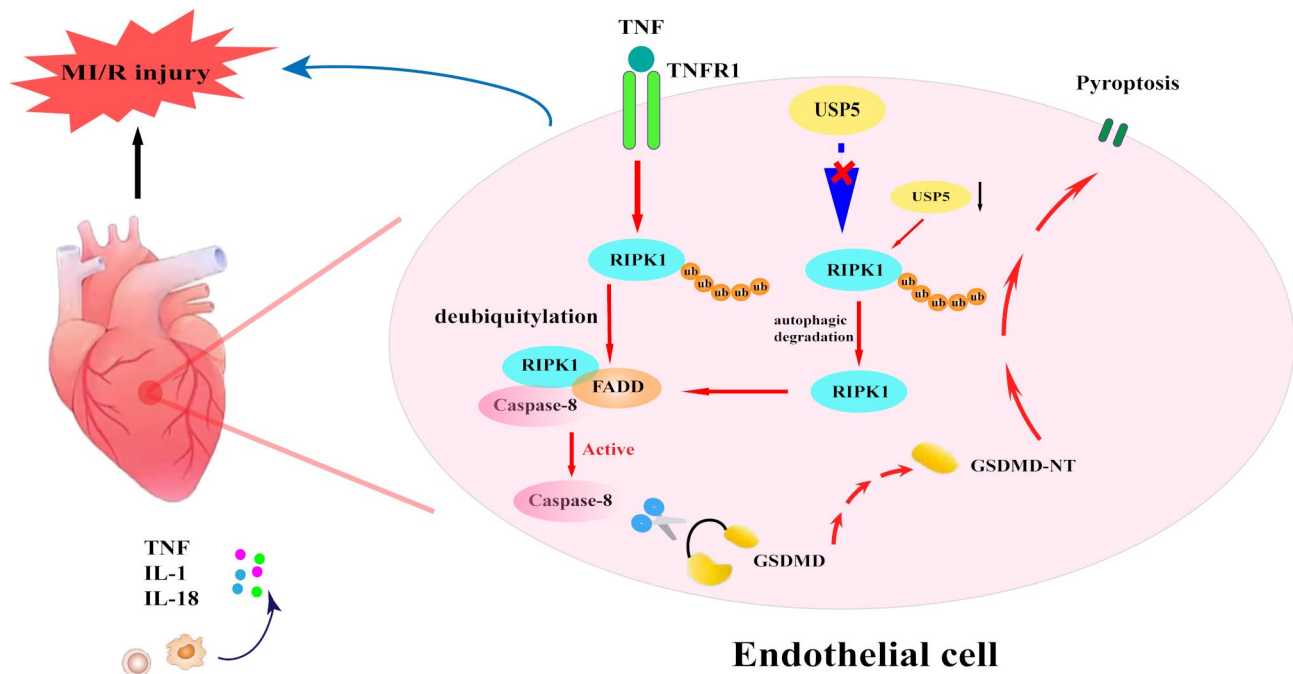
Fig. 7 Schematic model in which the USP5 deficiency inhibits MI/R-induced pyroptosis by suppressing RIPK1-mediated activation of caspase-8. Upon I/R, USP5 expression is upregulated, which subsequently inhibits K63-linked polyubiquitination of RIPK1 and promotes caspase-8 cleavage of gasdermin D to elicit pyroptosis. When USP5 is downregulated or mutated, RIPK1 reverse K63-linked deubiquitination, which leads to RIPK1 autophgic degradation and inhibits cell pyroptosis

of caspase-8 or RIPK3, promoting cell apoptosis or necrosis upon appropriate signals [18, 19]. Interestingly, recent studies indicate that apoptotic caspase-8 can directly cleave GSDMD to induce pyroptosis [20, 21]. Therefore, we hypothesize that RIPK1 may influence pyroptosis in cardiac microvascular endothelial cells (CMECs) by modulating caspase-8 cleavage of gasdermin D during I/R. Our results support this hypothesis, as downregulation of RIPK1 expression in endothelial cells in mice subjected to MI/R inhibited caspase-8 activity and pyroptosis. Furthermore, Cdh5-*Cre*$^{+}$/*RIPK1*$^{flox/flox}$ mice exhibited alleviated microvascular damage, reduced infarct size, myocardial or endothelial cell pyroptosis, and improved survival rate following MI/R. Additionally, these mice showed reduced inflammatory cell infiltration into the heart. These findings collectively indicate that RIPK1 deletion alleviates myocardial I/R injury by inhibiting pyroptotic cell death.

However, the precise molecular mechanism underlying RIPK1-mediated inhibition of pyroptosis remains poorly defined. Studies have reported that RIPK1, a key protein involved in cell death and inflammation, is highly regulated through various posttranslational modifications. One of the major mechanisms controlling RIPK1 is ubiquitination. As negative regulators, the E3 ligase TRAF2 facilitates RIPK1 polyubiquitination and prevents dendritic cell apoptosis

[22]. Similarly, PPDPF facilitates RIPK1 ubiquitination by recruiting the E3 ligase TRIM21, thereby inhibiting cell apoptosis and suppressing the development of hepatocellular carcinoma [23]. However, the physiological deubiquitinase that regulates RIPK1 stability remains elusive.

USP5 has been found to play vital roles in multiple cellular signaling pathways, such as in immune response [24], stress reactions [25], DNA repair [26], and cancer progression [27]. However, the role of USP5 in regulating pyroptosis has not been thoroughly investigated. In the present study, our results suggest that downregulated USP5 expression in the heart not only increases animal survival but also attenuates microvascular injury and myocardial infarct size post-MI/R. Moreover, USP5+/- mice exhibit increased susceptibility to promote capillary formation. Additionally, we observed lower levels of RIPK1 and GSDMD in heterozygous USP5+/- mice subjected to myocardial reperfusion-induced microvascular injury. Mechanistically, USP5 interacts with RIPK1, leading to deubiquitination and stabilization of RIPK1. Knockdown of USP5 greatly inhibits the interaction between USP5 and RIPK1, leading to increased degradation of RIPK1 by autophagy lysosomes. Based on the experimental data, we demonstrate that USP5 deficiency reverses K63-linked deubiquitination of RIPK1 and inhibits RIPK1-mediated pyroptosis. Thus, targeting

the USP5-RIPK1 axis could be a potential strategy for the treatment of microvascular injury subjected to MI/R.

Conclusion

In summary, our study reveals that downregulated USP5 expression in the heart exhibits an inhibitory effect on RIPK1-mediated pyroptosis by specifically reversing K63-linked deubiquitination of RIPK1 and suppressing CMECs pyroptosis. Our data uncover a crucial role of USP5 in protecting against microvascular damage by inhibiting RIPK1-mediated pyroptosis, suggesting that targeting USP5 might be a potential therapeutic approach for microvascular damage post-MI/R.

Supplementary Information

The online version contains supplementary material available at https://doi.org/10.1186/s12964-024-01853-x.

Supplementary Material 1

Data availability
No datasets were generated or analysed during the current study.

Declarations

Competing interests
The authors declare that they have no competing interests.

References
1. Correction to. Heart Disease and Stroke Statistics-2017 update: a Report from the American Heart Association. Circulation. 2017;136.
2. Heusch G. Myocardial ischaemia-reperfusion injury and cardioprotection in perspective. Nat Reviews Cardiol. 2020;17(12):773–89.
3. Xiang Q, Yi X, Zhu X, Wei X, Jiang D. Regulated cell death in myocardial ischemia-reperfusion injury. Trends Endocrinol Metab. 2024;35(3):219–34.
4. Shi H, Gao Y, Dong Z, Yang J, Gao R, Li X, et al. GSDMD-Mediated cardiomyocyte pyroptosis promotes myocardial I/R Injury. Circul Res. 2021;129(3):383–96.
5. He X, Fan X, Bai B, Lu N, Zhang S, Zhang L. Pyroptosis is a critical immune-inflammatory response involved in atherosclerosis. Pharmacol Res. 2021;165:105447.
6. Degterev A, Ofengeim D, Yuan J. Targeting RIPK1 for the treatment of human diseases. Proc Natl Acad Sci USA. 2019;116(20):9714–22.
7. Huyghe J, Priem D, Bertrand M. Cell death checkpoints in the TNF pathway. Trends Immunol. 2023;44(8):628–43.
8. Xu D, Jin T, Zhu H, Chen H, Ofengeim D, Zou C, et al. TBK1 suppresses RIPK1-Driven apoptosis and inflammation during development and in aging. Cell. 2018;174(6):1477–e9119.
9. Tao L, Yi Y, Chen Y, Zhang H, Orning P, Lien E, et al. RIP1 kinase activity promotes steatohepatitis through mediating cell death and inflammation in macrophages. Cell Death Differ. 2021;28(4):1418–33.
10. Peltzer N, Darding M, Walczak H. Holding RIPK1 on the Ubiquitin Leash in TNFR1 Signaling. Trends Cell Biol. 2016;26(6):445–61.
11. Wu B, Qiang L, Zhang Y, Fu Y, Zhao M, Lei Z, et al. The deubiquitinase OTUD1 inhibits colonic inflammation by suppressing RIPK1-mediated NF-κB signaling. Cell Mol Immunol. 2022;19(2):276–89.
12. Zhao Y, Huang J, Zhao K, Li M, Wang S. Ubiquitination and deubiquitination in the regulation of N-methyladenosine functional molecules. J Mol Med. 2024;102(3):337–51.
13. Kist M, Kőműves L, Goncharov T, Dugger D, Yu C, Roose-Girma M, et al. Impaired RIPK1 ubiquitination sensitizes mice to TNF toxicity and inflammatory cell death. Cell Death Differ. 2021;28(3):985–1000.
14. Schorn F, Werthenbach J, Hoffmann M, Daoud M, Stachelscheid J, Schiffmann L, et al. cIAPs control RIPK1 kinase activity-dependent and -independent cell death and tissue inflammation. EMBO J. 2023;42(22):e113614.
15. Sun W, Lu H, Dong S, Li R, Chu Y, Wang N, et al. Beclin1 controls caspase-4 inflammsome activation and pyroptosis in mouse myocardial reperfusion-induced microvascular injury. Cell Communication Signaling: CCS. 2021;19(1):107.
16. Qin X, Shan Y, Gao J, Li F, Guo Y. E3 ubiquitin ligase mind bomb 1 overexpression reduces apoptosis and inflammation of cardiac microvascular endothelial cells in coronary microvascular dysfunction. Cell Signal. 2022;91:110223.
17. Yanpiset P, Maneechote C, Sriwichaiin S, Siri-Angkul N, Chattipakorn S, Chattipakorn N. Gasdermin D-mediated pyroptosis in myocardial ischemia and reperfusion injury: cumulative evidence for future cardioprotective strategies. Acta Pharm Sinica B. 2023;13(1):29–53.
18. Liu C, Wang H, Han L, Zhu Y, Ni S, Zhi J, et al. Targeting P2YR protects against necroptosis of intestinal epithelial cells through PKA/CREB/RIPK1 axis in ulcerative colitis. Nat Commun. 2024;15(1):2083.
19. Lee C, Hwang G, Nam Y, Hwang C, Song J. IKK-mediated TRAF6 and RIPK1 interaction stifles cell death complex assembly leading to the suppression of TNF-α-induced cell death. Cell Death Differ. 2023;30(6):1575–84.
20. Demarco B, Grayczyk J, Bjanes E, Le Roy D, Tonnus W, Assenmacher C. Caspase-8-dependent gasdermin D cleavage promotes antimicrobial defense but confers susceptibility to TNF-induced lethality. Sci Adv. 2020; 6.
21. Sarhan J, Liu B, Muendlein H, Li P, Nilson R, Tang A, et al. Yersinia Caspase-8 induces cleavage of gasdermin D to elicit pyroptosis during infection. Proc Natl Acad Sci USA. 2018;115(46):E10888–97.
22. Harit K, Bhattacharjee R, Matuschewski K, Becker J, Kalinke U, Schlüter D, et al. The deubiquitinating enzyme OTUD7b protects dendritic cells from TNF-induced apoptosis by stabilizing the E3 ligase TRAF2. Cell Death Dis. 2023;14(7):480.
23. Wang Y, Ma N, Xu S, Huang J, Ni Q, Cao H, et al. PPDPF suppresses the development of hepatocellular carcinoma through TRIM21-mediated ubiquitination of RIPK1. Cell Rep. 2023;42(4):112340.
24. Ding L, Sun Y, Liang Y, Zhang J, Fu Z, Ren C et al. Beta-Cell Tipe1 Orchestrates Insulin Secretion and Cell Proliferation by Promoting Gαs/cAMP Signaling via USP5. Advanced science (Weinheim, Baden-Wurttemberg, Germany). 2024:e2304940.
25. Nostramo R, Varia S, Zhang B, Emerson M, Herman P. The Catalytic activity of the Ubp3 deubiquitinating protease is required for efficient stress Granule Assembly in Saccharomyces cerevisiae. Mol Cell Biol. 2016;36(1):173–83.
26. Xu X, Huang A, Cui X, Han K, Hou X, Wang Q, et al. Ubiquitin specific peptidase 5 regulates colorectal cancer cell growth by stabilizing Tu translation elongation factor. Theranostics. 2019;9(14):4208–20.
27. Li J, Wang Y, Luo Y, Liu Y, Yi Y, Li J, et al. USP5-Beclin 1 axis overrides p53-dependent senescence and drives Kras-induced tumorigenicity. Nat Commun. 2022;13(1):7799.